EPJ Photovoltaics **16**, 8 (2025)

https://doi.org/10.1051/epjpv/2024051

Available online at:
www.epj-pv.org

Special Issue on 'EU PVSEC 2024: State of the Art and Developments in Photovoltaics', edited by Robert Kenny and Gabriele Eder

ORIGINAL ARTICLE OPEN ACCESS

24% Efficient TOPCon-based back contacted polyZEBRA solar cells

Jonathan Linke*, Christoph Peter, Jan Hoß, Saman Sharbaf Kalaghichi, Valentin Mihailetchi, Jan Lossen, and Florian Buchholz

International Solar Energy Research Center Konstanz e.V., Rudolf-Diesel-Str. 15, 78467 Konstanz, Germany

Received: 16 July 2024 / Accepted: 3 December 2024

Abstract. This publication serves as an update on the progress of the back contacted polyZEBRA solar cell technology, which features Tunnel Oxide Passivating Contact (TOPCon) structures on both polarities. The solar cell efficiency mean values published by the end of last year have been improved by $+1\%_{abs}$ to 24.0%. Following the key parameter changes, it is discussed how this improvement has been achieved. These changes are in particular the cell thickness and base resistivity, a dedicated wet-chemical cleaning step, the rear AlO_x capping layer thickness and the pitch of the rear metallization pattern.

Keywords: polyZEBRA / back contact / IBC / TOPCon / poly-Si

1 Introduction

Industrial solar cell mass production currently undergoes the transition from the Passivated Emitter and Rear Cell (PERC) to the Tunnel Oxide Passivating Contact (TOPCon) technology [1]. Even though impressive improvements of the achieved solar cell conversion efficiencies have been reported in the last months [2], this technology will eventually be limited by the classically diffused front side. This limitation may be overcome by applying poly-Si/SiO_x TOPCon structures not only on the *n*-polarity, but also on the *p*-polarity. Due to the strong parasitic absorption of poly-Si layers [3,4], on the front side it has to be structured below the metal fingers [5–9]. Even more efficient is the application of both polarities poly-Si/SiO_x contacts on the rear side of the solar cell with a poly-Si free front side with no parasitic absorption at all. Such back contacted cell concepts were addressed in scientific literature already several years ago [10,11]. However, these concepts were not further developed towards industrial application, probably due to the applied high-cost photolithography technique for rear side patterning. Instead, it was decided to omit the TOPCon structure on the *p*-polarity and make use of a PERC-like local aluminum back surface field in the so-called POLO-IBC hybrid cell design [12]. In contrast, IBC cells featuring TOPCon structures on both polarities have already been established in the industry by Maxeon Solar Technologies (SunPower) and Aiko Solar. The challenge of back contacted solar cells is to reach cost-competitiveness to standard both side contacted solar cells, considering the complex requirements of the rear side patterning. Within the TOPCon-based back contacted polyZEBRA solar cell concept developed at ISC Konstanz [13] this challenge is tackled by using only industrially established low-cost equipment, i.e. laser patterning and screen-printing, in order to yield comparable $/kWh costs as standard both side contacted TOPCon technology.

In a previous publication from last year [14] a mean solar cell efficiency of ~23% was reported for the polyZEBRA cell concept along with simulations suggesting a roadmap to higher efficiencies. The present study serves as an update of the development progress and reports a recent mean value of 24.0% solar cell efficiency, which is $+1\%_{abs}$ compared to last year's publication. It is analyzed how this improvement has been achieved. In particular, the influence of the cell thickness and base resistivity, a dedicated wet-chemical cleaning step, the rear AlO_x capping layer thickness and the pitch of the rear metallization pattern is addressed.

2 Material and methods

For this study, polyZEBRA solar cells were fabricated according to the process flow shown in Figure 1, which is the same process flow used for fabrication of the solar cells discussed in last year's publication [14] and in all experiments in between. The base material were Cz-grown *n*-type wafers in M6 format with a thickness of 150 µm. On

* e-mail: jonathan.linke@isc-konstanz.de

the rear side, the emitter and base regions feature poly-Si/SiO_x contacts and are separated by a *p*-type diffused gap region. The interfacial tunnel oxides were thermally grown (~2 nm) and capped with low-pressure chemical vapor deposited (LPCVD) (n) poly-Si (Fig. 1, step 2) and (i) poly-Si (Fig. 1, step 6), respectively. A first BBr_3-diffusion was applied for the background *p*-type doping of the initially undoped (i) poly-Si and the resulting boron silicate glass (BSG) was removed in hydrofluoric acid (HF) (Fig. 1, step 7). The thermal budget (965 °C) of the second BBr_3-diffusion for *p*-type doping of the gap and front side region also activates the passivation of the poly-Si/SiO_x structures on both polarities (Fig. 1, step 10). Details regarding the laser-based patterning steps (Fig. 1, step 4, 8) can be found in [15,16]. Plasma-enhanced chemical vapor deposited (PECVD) stacks of AlO_x capped with a SiN_x layer were used for passivation of the surfaces. The metal contacts were screen-printed with Ag-containing paste for both fingers and busbars (BB) and a pitch of the rear metallization pattern of 800 µm and 6BB.

Alongside with the cells, all experiments include reference wafers which follow the exact same process, but the laser patterning of the rear side creates 40×40 mm^2 squares of the individual cell regions (n poly-Si/SiO_x, p poly-Si/SiO_x, gap/front side) instead of the narrow straight line pattern for the cells. These squares enable characterization methods, which would not be applicable to the lines as thin as 500 µm. In order to separate the effect of single parameter changes, results of further experiments are shown, in which a specific parameter change was explicitly tested against a dedicated control group.

In last year's publication, different cappings of the rear AlO_x passivation were tested, namely "Capping A" as control group and "Capping B" with improved capping. The group with improved capping showed higher cell efficiencies, but nevertheless, all results of the present study are compared to the control group of last year's publication. The reason is that the improved capping showed much worse passivation quality on cell precursors before metallization, an issue that could not be fixed until now. In this sense, all improvements of the present study are benchmarked against this control group of [14].

Table 1 shows the differences in experimental parameters between last year's control group and the cells from the present study. The final cell thickness is a bit thinner due to thinner as-delivered wafers and optimizations of the alkaline etching steps throughout the process. One outcome of last year's study supported to use wafers with a lower base resistivity as the loss in current was overcompensated by a gain in fill factor. Thus, also a lower base resistivity was chosen for the present study. Another difference is the omitting of a dedicated cleaning after alkaline texturing in addition to the standard cleaning. In order to reduce last year's strong recombination below the metal-semiconductor interfaces, the thickness of the rear AlO_x capping has been increased with the goal to minimize spiking of the metal through the interfacial oxide of the poly-Si/SiO_x structure. In addition, the pitch of the rear side metallization pattern was reduced, which increases the density of fingers and thus increases the charge carrier collection efficiency. It should be noted that

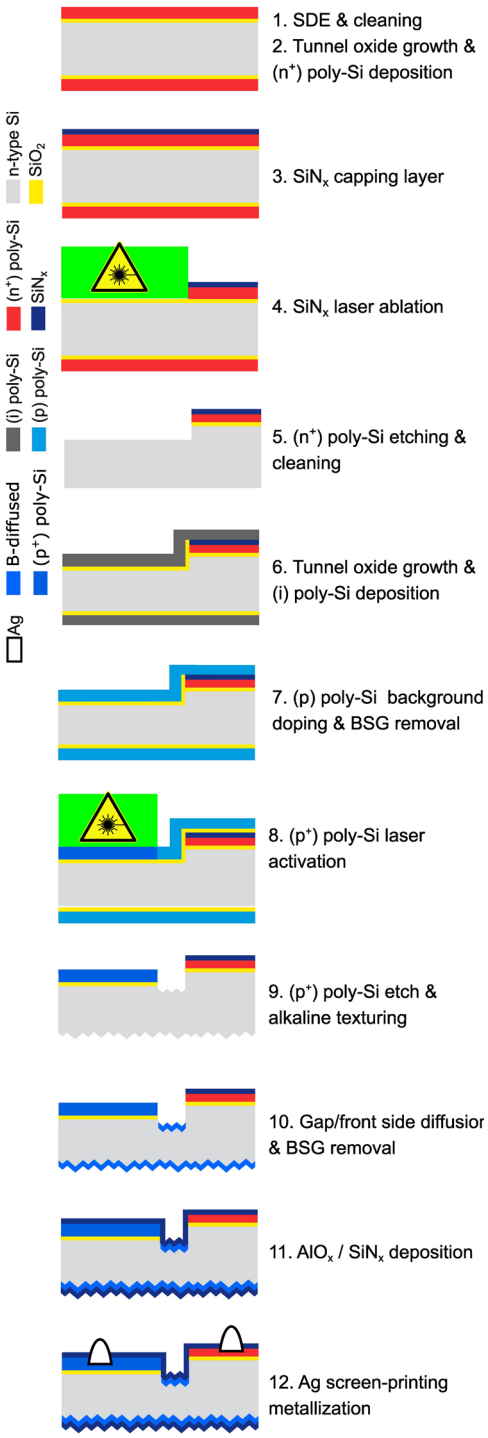

Fig. 1. PolyZEBRA solar cell fabrication process flow based on [13].

the thermal budget and interfacial oxide thicknesses, whose tuning is of high relevance for poly-Si/SiO_x structures, has not been altered since last year's publication and was the same in all experiments presented in this contribution.

The IV curves of the solar cells were recorded using a conventional Halm flasher. The individual regions of the cells were characterized by quasi steady-state photoconductance (QSSPC) measurements with a Sinton

Table 1. Differences in experimental parameters of the control groups of last year's publication [14] and of this study.

Experimental parameter	Last year's publication [14]	Present study
Cell thickness after process	~145 µm	~135 µm
Base resistivity	~13 Ωcm	~4 Ωcm
Dedicated cleaning after texture	Yes	No
Rear AlO_x capping thickness	~60 nm	~75 nm
Cell pitch	1080 µm	800 µm

Table 2. Most important simulation input parameters based on measurement data of test structures, which represent the process flow and parameters used for the fabrication of the solar cells.

	Input parameter	Value
General properties	Wafer size	M6
	#BB	6BB
	τ_{bulk}	3 ms
Rear pattern	Pitch	800 µm
	W_{base}	290 µm
	W_{emi}	360 µm
	W_{gap}	75 µm
Surface recombination	$J_{0,pass,\ (n)\ poly\text{-}Si}$	1 fA/cm^2
	$J_{0,pass,\ (p)\ poly\text{-}Si}$	10 fA/cm^2
	$J_{0,pass,gap/front}$	13 fA/cm^2
Metal recombination	$J_{0,met,\ (n)\ poly\text{-}Si}$	50 fA/cm^2
	$J_{0,met,\ (p)\ poly\text{-}Si}$	500 fA/cm^2
Sheet resistance	$R_{sheet,\ (n)\ poly\text{-}Si}$	55 Ω/sq
	$R_{sheet,\ (p)\ poly\text{-}Si}$	175 Ω/sq
	$R_{sheet,gap/front}$	490 Ω/sq
Resistivity	$\rho_{c,\ (n)\ poly\text{-}Si}$	0.9 mΩcm^2
	$\rho_{c,\ (p)\ poly\text{-}Si}$	2.8 mΩcm^2

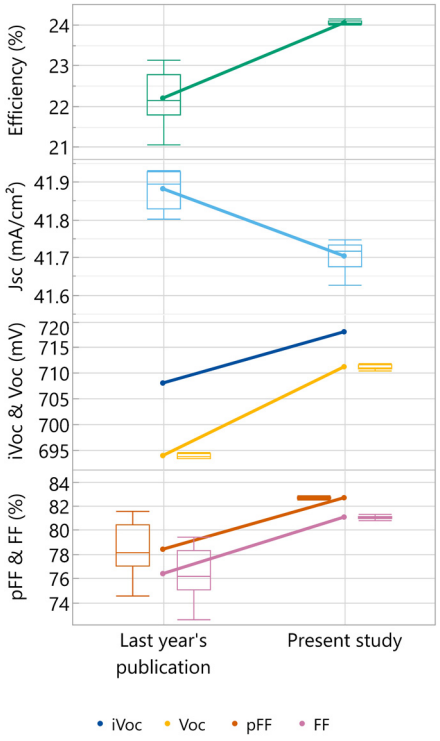

Fig. 2. Solar cell parameters determined by IV measurements of the polyZEBRA cells from last year's publication [14] and the present study. The iV_{oc} values were taken from QSSPC measurements on cell precursors before metallization.

Lifetime Tester on the reference wafers featuring the squares as described above. Additionally, some cells were excluded as precursors before metallization in order to enable QSSPC measurements on the actual IBC pattern.

The experimental data is supported by simulations done with Quokka3 [17]. The most important input parameters are based on measurement data of test structures, which reflect the process flow and parameters used for the fabrication of the solar cells (Fig. 1). They are listed in Table 2. The bulk lifetime (τ_{bulk}) was adjusted in order to match the simulated open-circuit voltage (V_{oc}) to the experimentally determined implied open-circuit voltage (iV_{oc}) with the metal recombination turned off. Subsequently, the metal recombination of the (n) poly-Si/SiO_x was fixed to 50 fA/cm^2 while the metal recombination of the (p) poly-Si/SiO_x was adjusted in order to match the simulated V_{oc} to the experimentally determined V_{oc}.

3 Results and discussion

Figure 2 shows the IV data of the solar cells and iV_{oc} values of the cell precursors before metallization of last year's publication and of the present study. First of all it is evident, that the scattering of the fill factor (FF) data from last year's publication is much larger. This is attributed to contacting problems with the IV measurement chuck, which have been solved in the meantime.

All cell parameters show significant improvement apart from the short circuit current density J_{sc}. The differences in the mean values are +1.8%$_{abs}$ in cell efficiency, −0.2 mA/cm^2 in J_{sc}, +10 mV in iV_{oc}, +17mV in V_{oc}, +4.3%$_{abs}$ in pFF and +4.7%$_{abs}$ in FF. Furthermore, the iV_{oc}-to-V_{oc} loss,

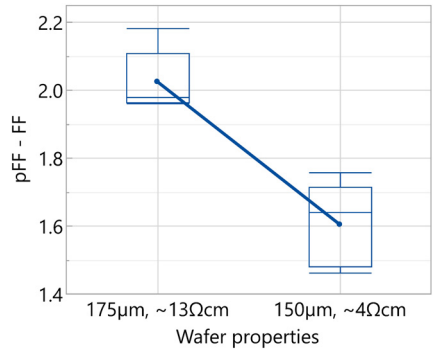

Fig. 3. pFF-to-FF loss as a measure for the cell's series resistance R_{ser} as function of wafer thickness and resistivity from last year's publication [14] (175 µm, ~13 Ωcm) and the present study (150 µm, ~4 Ωcm).

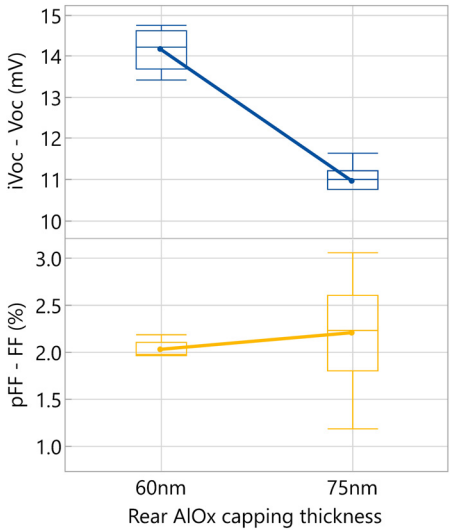

Fig. 4. iV_{oc}-to-V_{oc} loss as a measure for the recombination at the metal-semiconductor interfaces $J_{0,met}$ and pFF-to-FF loss as a measure for the cell's series resistance R_{ser} for a rear AlO_x capping thickness of 60 nm in last year's publication [13] and a follow-up experiment with ~15 nm thicker capping.

which serves as a measure for the total recombination at the metal-semiconductor interfaces, was decreased by −7 mV and the pFF-to-FF loss, which serves as a measure for the series resistance R_{ser}, was reduced by $-0.4\%_{abs}$. In the following it is discussed, how the changes in experimental parameters as summarized in Table 1 can explain these differences in the cells' IV data.

3.1 Wafer thickness and base resistivity

The wafers of last year's publication and the present study were provided by different suppliers with different characteristics. The wafers used in the present study were thinner as-delivered with 150 µm compared to 175 µm before. Furthermore, the base resistivity was lower with ~4 Ωcm compared to ~13 Ωcm, a choice which was taken based on the lower series resistance that is expected from lower resistivity wafers in [14,18]. From simulations the thinner wafer would cause a loss in J_{sc} of $\sim 0.03\,mA/cm^2$ and the lower base resistivity a loss of $\sim 0.18\,mA/cm^2$, which in sum is able to explain the experimentally observed loss of $\sim 0.2\,mA/cm^2$.

A lower base resistivity also implies a lower series resistance, which is experimentally accessible via the smaller pFF-to-FF loss, as shown in Figure 3. It has reduced from $\sim 2\%_{abs}$ to $\sim 1.6\%_{abs}$, which corresponds to a relative reduction of 20%. However, from the simulation the series resistance is reduced by only 2.5%, so other effects seem to be contributing to the lower series resistance as will be discussed in the upcoming sections.

3.2 Dedicated cleaning after texture

Due to historical reasons from the development of the process sequence a dedicated cleaning process after alkaline texture was used in addition to the standard pSC1 (KOH/H_2O_2) and HF/HCl clean. In this additional step, the wafers were rinsed in HF/HCl once again, dipped for 10 min into piranha solution (H_2SO_4/H_2O_2 mixture) at elevated temperature and the resulting oxide was stripped in HF. Since such additional cleaning is uncommon, especially from an industrial point of view, it was tested to skip it. The cells without additional cleaning showed a ~3 mV higher V_{oc} compared to the control group, which was also confirmed by the iV_{oc} of cell precursors before metallization. QSSPC measurements on the reference wafers featuring squares of the individual regions revealed, that this improvement in iV_{oc} occurs only on the (p) poly-Si/SiO_x regions while the (n) poly-Si/SiO_x and the gap/front side regions are unaffected. We speculate that the (p) poly-Si layers has some pinholes through which the etch solution could reach and damage the buried interfacial oxide. If so, all wet chemical steps should be kept to a minimum duration and thus skipping the additional cleaning showed a beneficial effect.

3.3 Rear AlO_x capping thickness

The rear side of a back contacted cell is commonly covered by a large metal fraction as well as by a large fraction of heavily light absorbing poly-Si layers [3,4]. Hence, bifaciality plays a minor role and so the capping of the rear AlO_x does not necessarily have to be optimized towards optimum light trapping. On the other hand, the properties of the capping significantly influence the metallization, as also discussed in [14,19,20]. In particular, the thickness is expected to influence both the recombination current density at the metal-semiconductor interfaces $J_{0,met}$ as well as the series resistance R_{ser}. Figure 4 shows the iV_{oc}-to-V_{oc} loss as measure for $J_{0,met}$ and the pFF-to-FF loss as measure for R_{ser} for the capping thickness applied in last year's publication and for a ~15 nm thicker capping.

The iV_{oc}-to-V_{oc} loss decreases by ~3 mV for the thicker mask, meaning that the $J_{0,met}$ is reduced. A similar decreasing $J_{0,met}$ for thicker dielectric stack was reported before [20]. As the firing conditions were the same, this

Table 3. Differences in emitter, base and gap widths under reduction of the pitch of the rear metallization.

	Last year's publication [14]	Present study
Pitch	1080 µm	800 µm
Emitter width	570 µm	360 µm
Base width	290 µm	290 µm
Gap width	110 µm	75 µm

phenomenon is explained by a larger amount of SiN_x capping to be etched by the paste, which reduces the total area of metal inside the poly-Si layer. And this in turn implies a lower area of damaged or penetrated interfacial oxide, eventually reducing the $J_{0,met}$ and increasing the V_{oc}.

Based on this reasoning, an increase in R_{ser} is expected from the higher contact resistance from the lower amount of metal in the poly-Si layer. This increase in R_{ser} is reflected in the ~0.2%$_{abs}$ higher mean and median pFF-to-FF loss values for the thicker capping (Fig. 4), though the scattering is large. It is expected however, that the gain in V_{oc} will overcompensate the slightly higher R_{ser}. Unfortunately, it was not possible to validate this hypothesis with the achieved cell efficiencies, as the group with thicker capping showed a much lower J_{sc} than the control group, which is not a consequence of the thicker capping as confirmed by a follow-up experiment.

3.4 Pitch of rear metallization pattern

The pitch of the rear metallization pattern determines the total number of fingers on the cell. This in turn influences the charge carrier collection [18], the total recombination current at the metal-semiconductor interfaces and the light reflection on the rear side and as such the bifaciality. In order to boost the charge carrier collection and decrease the series resistance, the pitch was reduced from 1080 µm in last year's publication to 800 µm without changing the finger dimensions. The corresponding changes in the emitter, base and gap widths are listed in Table 3. The effects on the iV_{oc}-to-V_{oc} loss and the pFF-to-FF loss are shown in Figure 5.

On the one hand, the pFF-to-FF loss as a measure for R_{ser} is significantly reduced with the smaller pitch to less than 50% of the value of the control group. Due to the smaller distance between two fingers of the same polarity, the charge carriers need to travel a shorter distance until they are collected by the fingers and so the series resistance reduces. This effect is mostly responsible for the reduction of pFF-to-FF loss between last year's publication and the present study as presented in Figure 3.

On the other hand, the larger number of fingers causes a larger total area of metal-semiconductor interfaces from spiking through the interfacial oxide and in turn a higher

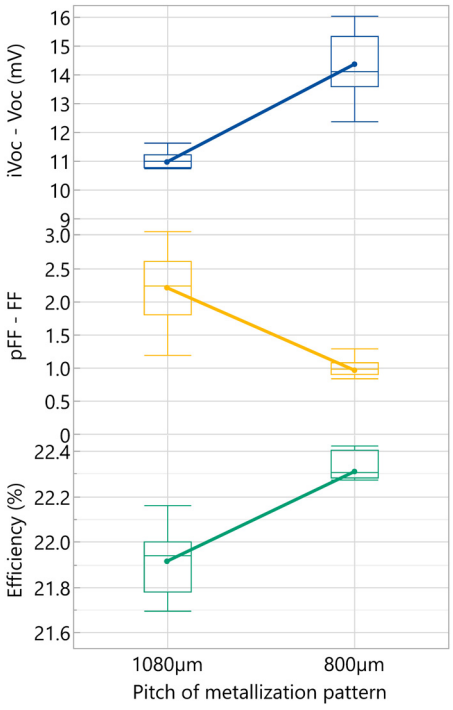

Fig. 5. iV_{oc}-to-V_{oc} loss as a measure for the recombination at the metal-semiconductor interfaces $J_{0,met}$, pFF-to-FF loss as a measure for the cell's series resistance R_{ser} and solar cell efficiency from an intermediate experiment comparing the pitch of the rear metallization pattern of 1080 µm as used in last year's publication [14] to a smaller pitch of 800 µm as used in the present study.

total recombination current in the whole cell. This effect materializes for the smaller pitch in +4 mV of the iV_{oc}-to-V_{oc} loss as a measure for the total recombination current.

Nevertheless, as the solar cell efficiency is ~0.4%$_{abs}$ higher for the pitch of 800 µm, the gain in R_{ser} overcompensated the loss in $J_{0,met}$.

3.5 Remaining parameter gains

The above described explicit changes in process parameters can explain the gain in cell efficiency only partly. For instance, the iV_{oc} of the cell precursors before metallization has improved by +10 mV, even though the dedicated cleaning after texture did only yield +3 mV. Also, the iV_{oc}-to-V_{oc} loss was reduced by 7 mV from 14 to 7 mV, but the decrease caused by the thicker rear AlO_x capping (Fig. 4) and the increase caused by the lowered pitch of the rear metallization pattern (Fig. 5) just cancel each other out. Since last year's publication and the present study 14 cell batches with 100 wafers each have been processed. As nearly the entire wafer handling was done manually, such a large number of batches leads to a learning curve of the operators. Also, minor changes to individual process parameters without explicit tests against a control group probably also have improved the iV_{oc} Another potential contribution is an improved wafer quality from recent deliveries.

Another beneficial effect could have been the change towards a four times larger laser spot from $30 \times 30\,\mu m^2$ to $30 \times 130\,\mu m^2$ rectangular top-hat geometry. Laser top-hat spot edges typically provide less fluence to the substrate than the homogenous bulk of the spot, an issue that was addressed by a certain overlap of neighboring spots. For the larger spot the area fraction of these overlapping regions is lower because of the lower edge-to-bulk ratio. Assuming a locally worse passivation in these overlapped regions, the reduced area fraction of the overlapping regions of the larger spot could have increased the iV_{oc}.

But also the other way round, the strong reduction in pFF-to-FF loss by more than 50% from the smaller pitch (Fig. 5) suggests a much larger reduction than has been observed between last year's publication and the present study (Fig. 3). However, the large scattering of the data of the control group weakens the meaningfulness of the 50% reduction, which is based on a comparison of the mean values. Simulations with the smaller pitch support this interpretation with a predicted R_{ser} reduction of ~30%, which is closer to the 20% reduction experimentally observed between last year's publication and the present study.

4 Conclusion and outlook

The polyZEBRA solar cell efficiency mean value of 23.0% from last year's publication was improved by $1\%_{abs}$. to 24.0%. The major changes of the process parameters were analyzed, but are not consistently able to explain all the parameter gains. The remaining improvements are attributed to a general learning curve of the manual processing steps and minor parameter adjustments without explicit control groups. Next steps to further boost the cell efficiency are the minimization of the iV_{oc}-to-V_{oc} loss while maintaining the high FF by an improved metallization sequence and the general increase of the passivation of the individual regions of the cell, i.e. the minimization of the recombination $J_{0,pass}$ on the front side, in order to increase the V_{oc}.

Acknowledgments

The authors would like to thank all colleagues at ISC Konstanz that have contributed indirectly in the laboratory and administration as an essential part of the research process and functionality of the institute.

Funding

This work was supported by the project "IBC4EU" and has received funding from the European Union's Horizon Europe research and innovation programme under grant agreement No. 101084259.

Conflicts of interest

The authors have nothing to disclose.

Data availability statement

Reported data can be provided upon request.

Author contribution statement

Conceptualization: J.Li., C.P. and F.B.; Methodology: J.Li., C.P. and F.B.; Validation, J.Li., C.P., J.H., S.S.K., V.M. and F.B.; Formal Analysis: J.Li. and C.P.; Investigation: J.Li., C.P. and S. S.K.; Resources: F.B.; Data Curation: J.Li., C.P. and F.B.; Writing – Original Draft Preparation: J.Li.; Writing – Review & Editing: J.Li., C.P., J.H., S.S.K., V.M., J.Lo. and F.B.; Supervision: J.Lo. and F.B.; Project Administration: F.B.; Funding Acquisition: F.B. All authors have read and agreed to the published version of the manuscript.

References

1. M. Fischer, M. Woodhouse, P. Baliozian, International Technology Roadmap for Photovoltaics (ITRPV) 2023 Results, VDMA Photovoltaics Equipment, 15th Edition (2024). https://www.vdma.org/international-technology-roadmap-photovoltaic
2. A. Mette, S. Hörnlein, F. Stenzel, R. Hönig, I. Höger, M. Schaper, K. Petter, M. Junghänel, C. Klenke, A. Weihrauch, H.-C. Ploigt, O. Kwon, A. Schönmann, O. Tobail, K. Kim, A. Schwabedissen, M. Kauert, K. Duncker, B. Faulwetter-Quandt, J. Scharf, J. Cieslak, F. Kersten, B. Lee, S. T. Kristensen, O. Schnelting, C. Baer, M. Queck, G. Zimmermann, L. Burtone, L. Niebergall, M. Schütze, S. Schulz, M. Fischer, S. Peters, F. Fertig, J. W. Müller, Q. ANTUM NEO with LECO Exceeding 25.5% cell Efficiency, Sol. Energy Mater. Sol. Cells **277**, 113110 (2024). https://doi.org/10.1016/j.solmat.2024.113110
3. J. Steffens, Dependencies between poly-Si composition and solar cell performance of poly-Si/SiOx passivating contacts, Ph.D. thesis, Universität Konstanz, Konstanz, Germany, 2020. http://nbn-resolving.de/urn:nbn:de:bsz:352-2-19tzla6vns71f7
4. F. Feldmann, M. Nicolai, R. Müller, C. Reichel, M. Hermle, Optical and electrical characterization of poly-Si/SiOx contacts and their implications on solar cell design, Energy Procedia, **124**, 31 (2017). https://doi.org/10.1016/j.egypro.2017.09.336
5. J. Hoß, S.S. Kalaghichi, M. Comak, P. Preis, J. Lossen, J. Linke, L. Koduvelikulathu, F. Buchholz, Advanced TOPCon solar cells with vanishing metal induced recombination losses, EPJ Photovolt. **15**, 43 (2024). https://doi.org/10.1051/epjpv/2024040

6. S.-P. Hsu, C.-P. Huang, K.-C. (Jay)Lai, C.-C. Li, B.-C. Kung, S.-Y. Chen, M.-T. Kuo, H.-C. Chang, Localized bifacial passivated contacts solar cell with 23.5% efficiency, in *Proc. of 40th European Photovoltaic Solar Energy Conference and Exhibition EUPVSEC* (Lisbon, 2023), p. 020042. https://doi.org/10.4229/EUPVSEC2023/1CV.3.1
7. F. Meyer, A. Ingenito, J. J. Diaz Leon, X. Niquille, C. Allebé, S. Nicolay, F.-J. Haug, C. Ballif, Localisation of front side passivating contacts for direct metallisation of high-efficiency c-Si solar cells, Sol. Energy Mater. Sol. Cells **235**, 111455 (2022). https://doi.org/10.1016/j.solmat.2021.111455
8. J. Wang, S.P. Phang, T.N. Truong, Z. Li, H.T. Nguyen, D. Macdonald, J. Stuckelberger, Inkjet-printed boron-doped poly-Si/SiOx passivating contacts, Sol. Energy Mater. Sol. Cells **272**, 112928 (2024). https://doi.org/10.1016/j.solmat.2024.112928
9. B. Uygun, S. Kluska, J.-I. Polzin, J. Schube, M. Jahn, K. Krieg, R. Turan, H. Nasser, Local p+ Poly-Si passivating contacts realized by direct FlexTrail printing of boron ink and selective alkaline etching for high efficiency TOPCon based solar cells, Authorea (2024). https://doi.org/10.22541/au.172114744.47084956/v1
10. F. Haase, C. Hollemann, S. Schäfer, A. Merkle, M. Rienäcker, J. Krügener, R. Brendel, R. Peibst, Laser contact openings for local poly-Si-metal contacts enabling 26.1%-efficient POLO-IBC solar cells, Sol. Energy Mater. Sol. Cells, **186**, 184 (2018). https://doi.org/10.1016/j.solmat.2018.06.020
11. G. Yang, P. Guo, P. Procel, G. Limodio, A. Weeber, O. Isabella, M. Zeman, High-efficiency black IBC c-Si solar cells with poly-Si as carrier-selective passivating contacts, Sol. Energy Mater. Sol. Cells, **186**, 913 (2018). https://doi.org/10.1016/j.solmat.2018.06.019
12. F. Haase, C. Hollemann, S. Schafer, J. Krugener, R. Brendel, R. Peibst, Transferring the record *p*-type Si POLO-IBC cell technology towards an industrial level, in *IEEE 46th Photovoltaic Specialists Conference (PVSC)* (Chicago, IL, USA, 2019), p. 2200. https://doi.org/10.1109/PVSC40753.2019.8980960
13. J. Linke, F. Buchholz, V. Mihailetchi, C. Peter, J. Hoß, J. Lossen, R. Kopecek, Fully passivating contact IBC solar cells using laser processing, in *Proc. of 8th World Conference on Photovoltaic Energy Conversion WCPEC* (Milan, Italy, 2022), p. 102. https://doi.org/10.4229/WCPEC-82022-1CV.2.11
14. J. Linke, F. Buchholz, S. Sharbaf, J. Hoß, V. Mihailetchi, J. Lossen, R. Kopecek, Progress in development of polyZEBRA IBC solar cells, in *Proc. of 40th European Photovoltaic Solar Energy Conference and Exhibition EUPVSEC* (Lisbon, Portugal, 2023) p. 020046. https://doi.org/10.4229/EUPVSEC2023/1CV.3.3
15. F. Buchholz, J. Linke, J. Hoss, H. Chu, V. Mihailetchi, A. Chaudhary, J. Lossen, R. Kopecek, E. Wefringhaus, Local passivating contacts from laser doped p+ polysilicon, in *Proc. of 38th European Photovoltaic Solar Energy Conference and Exhibition EUPVSEC* (Online, 2021), p. 140. https://doi.org/10.4229/EUPVSEC20212021-2BO.11.3
16. S. Sharbaf Kalaghichi, J. Hoß, R. Zapf-Gottwick, J.H. Werner, Laser activation for highly boron-doped passivated contacts, Solar **3**, 362 (2023). https://doi.org/10.3390/solar3030021
17. A. Fell, Quokka3, v2.4.6. (2024), www.quokka3.com
18. K.R. McIntosh, M.J. Cudzinovic, D.D. Smith, W.P. Mulligan, R.M. Swanson, The choice of silicon wafer for the production of low-cost rear-contact solar cells, in *Proc. of 3rd World Conference on Photovoltaic Energy Conversion WCPEC* (Osaka, Japan, 2003), p. 971
19. J. Linke, F. Buchholz, C. Peter, J. Hoß, J. Lossen, R. Kopecek, The role of masking layers during metallization of poly-Si/SiOx contacts, in *Proc. of Silicon PV 2022* (Konstanz, Germany, 2023), p. 02004. https://doi.org/10.1063/5.0141842
20. V.D. Mihailetchi, H. Chu, R. Kopecek, Insight into metal induced recombination losses and contact resistance in industrial silicon solar cells, in *Proc. of 7th World Conference on Photovoltaic Energy Conversion WCPEC* (Waikoloa Village, HI, 2018), p. 2673. https://doi.org/10.1109/PVSC.2018.8547888

Cite this article as: Jonathan Linke, Christoph Peter, Jan Hoß, Saman Sharbaf Kalaghichi, Valentin Mihailetchi, Jan Lossen, Florian Buchholz, 24% Efficient TOPCon-based back contacted polyZEBRA solar cells, EPJ Photovoltaics **16**, 8 (2025)